*Journal of the American Ceramic Society*

RESEARCH ARTICLE OPEN ACCESS

# Thermally Activated Deformation Mechanisms in MgO Investigated via High Temperature Scanning Indentation

Marcel Sos[1] | Oliver Preuß[2,3] | Sebastian Bruns[1] | Karsten Durst[1]

[1]Technical University Darmstadt, Physical Metallurgy, Darmstadt, Germany | [2]Technical University Darmstadt, Nonmetallic-Inorganic Materials, Darmstadt, Germany | [3]Karlsruhe Institute of Technology, Institute For Applied Materials, Karlsruhe, Germany

**Correspondence:** Marcel Sos (marcel.sos@tu-darmstadt.de)

**Received:** 23 April 2026 | **Revised:** 23 June 2026 | **Accepted:** 24 June 2026

**Keywords:** deformation mechanism | dislocation | high temperature | MgO | nanoindentation

## ABSTRACT

Magnesium oxide (MgO) serves as a model material for plastically deformable ceramics. In previous studies, it has mainly been investigated via uniaxial compression, with studies often focusing on a particular deformation mechanism and temperature range. In this work, the novel high temperature scanning indentation (HTSI) nanoindentation method is applied to characterize the mechanical properties of single-crystalline MgO from room temperature to 800°C, allowing a quasi-continuous measurement of hardness, elastic modulus, the coefficient of strain rate sensitivity, and the activation volume.

Results show that the hardness is controlled by hard 1/2<110>{100} slip, while the activation parameters are influenced by both 1/2<110>{100} and 1/2<110>{110} slip systems. The temperature dependence of the hardness follows two linear regimes, while the strain rate sensitivity shows complex behavior with a maximum of $m = 0.05$ at a temperature of 675°C. In the same regime, the activation volume remains approximately constant at $V = 10$–$20\ b^3$. At higher temperatures, it increases to $V = 100\ b^3$. The combined hardness and activation parameter data enable the determination of transition temperatures between different deformation regimes. With increasing temperature, MgO first shifts from a kink-pair to an obstacle-controlled regime at 240°C, with long-range dislocation interactions setting in at higher temperatures above 675°C.

## 1 | Introduction

Recent years have seen a renewed interest in the investigation of dislocations in ceramics [1–4]. This not only includes functional properties, but also aims to modify the mechanical properties by changing the dislocation density to ensure longevity of future functional devices [5, 6]. One model material for the investigation of dislocations and plasticity in ceramics is MgO, which can be plastically deformed down to cryogenic temperatures [7].

Its temperature-dependent mechanical properties and deformation mechanisms have mostly been studied in the latter half of the 20th century [8–10]. The key findings of those investigations are summarized in-depth in Messerschmidt's 2010 book [11] and a 2018 review by Amodeo et al. [12].

In literature, most tests were performed via macroscopic uniaxial compression of single crystals. The yield strength of MgO strongly depends on both temperature and crystal orientation [13, 14]. This can be attributed to the available slip systems. Due to the positions of the ions in the unit cell, slip without equal charges in close proximity during intermediate states is only possible with a Burgers vector of $b = 1/2<110>$ [9, 15]. The soft 1/2<110>{110} slip system shows a strong decline in critical resolved shear stress (CRSS) from low to intermediate temperatures, with reported athermal transition temperatures $T_A$ on the order of 500–700 K [11, 12, 16, 17]. Values of $CRSS_{\{110\}}$ ranging from 20–60 MPa have

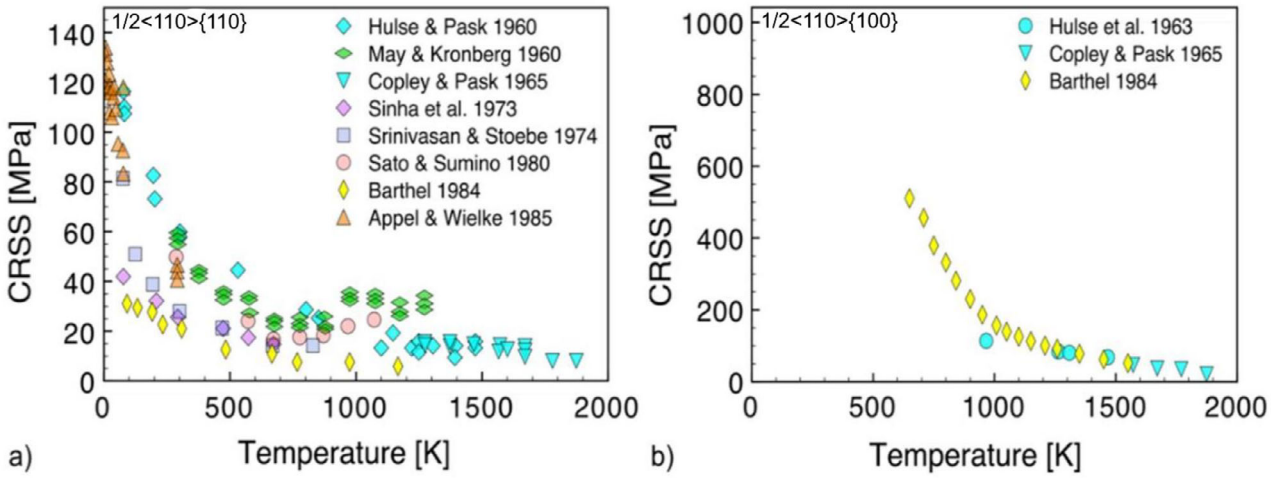


**FIGURE 1** | Experimental values of the CRSS of the 1/2<110>{110} (a) and 1/2<110>{100} (b) slip systems. *Source:* Reproduced from [12] under the CC BY 4.0 license.

been reported at room temperature, resulting in a yield stress of 40–120 MPa for [100] compression (Figure 1a). Deformation on the 1/2<110>{110} slip system is reported to be governed by the kink-pair mechanism, as well as localized obstacles and impurity hardening [11, 18, 19].

At higher temperatures, slip on the hard 1/2<110>{100} system also becomes possible. Its CRSS is significantly higher and strongly decreases up to temperatures of around 1000 K [12–14] (Figure 1b).

Despite the low yield stress when a sample is compressed in the [100] orientation, the indentation hardness is significantly higher than what an estimate via $H \approx 3 * \sigma_y$ would suggest reaching values on the order of 8–10 GPa [20–22]. This discrepancy arises due to the rock salt structure, which possesses six physical, but only two independent 1/2<110>{110} slip systems [23, 24]. This necessitates slip on secondary systems to accommodate the more complex deformation below the indenter. The relation between uniaxial and indentation tests is discussed in detail in Section 3.2.

More recent publications on MgO have dealt with deformation at high temperatures and high pressure, aiming to better describe deformation in the Earth's mantle [16, 25, 26]. Most indentation studies on MgO have focused on incipient plasticity and the dislocation structure around the indent [27–30], and the strain rate sensitivity or stress exponent have largely only been investigated at temperatures beyond 1000°C via macroscopic creep experiments [31–33].

This work aims to characterize the temperature-dependent mechanical properties of MgO using the novel high temperature scanning indentation (HTSI) nanoindentation method [34] to demonstrate the applicability of modern nanoindentation methods for the investigation of ductile ceramics, as recent developments in dislocation engineering [5] necessitate the determination of local mechanical properties in areas with different dislocation densities.

During an HTSI measurement, high-speed indentations on the order of 1 s per indent are carried out while heating the sample, enabling the quasi-continuous measurement of the hardness and elastic modulus. Furthermore, by analyzing a relaxation segment at the maximum load, the coefficient of strain rate sensitivity and the activation volume can be determined as a function of temperature, which can provide insight into thermally activated deformation mechanisms [35–37]. HTSI experiments are performed on single-crystalline (100)-oriented MgO from room temperature to 800°C, recording data at a resolution of 1 indent per 3°C.

The obtained results are discussed with respect to activity on the soft and hard slip systems and the underlying deformation mechanisms.

## 2 | Experimental Methodology

A single-crystalline single-sided polished (100) $10 \times 10 \times 1.5$ mm$^3$ MgO wafer was purchased from Alineason Materials Technology GmbH (Frankfurt am Main, Germany). The rear surface was subsequently mechanically ground up to 4000-grit paper. The roughness of the tested surface was measured via an Olympus LEXT OLS4100 confocal laser scanning microscope (Waltham, MA, USA) as $R_a \approx$4–6 nm.

The high temperature nanoindentation experiments were performed using a KLA HT1K "Prometheus" (Milpitas, CA, USA) ultra-high temperature nanoindenter [38] equipped with a diamond Berkovich tip (Synton-MDP AG, Nidau, Switzerland). The indenter assembly was mounted inside a TESCAN VEGA3 SEM (Brno, Czech Republic), and testing was carried out in vacuum ($p < 1\times10^{-3}$ Pa). Before testing, the tip area function was calibrated on fused silica according to Oliver and Pharr [39]. The temperature matching procedure for the HTSI measurement was performed at 400°C according to Minnert et al. [38].

The HTSI measurement cycle was performed with a tip and sample heating rate of 3°C/min and 3.47°C/min, respectively, up to a tip temperature of 800°C and a corresponding sample mount temperature of 922.2°C. The chosen heating rates enabled an approximate equilibrium of tip and sample surface temperature

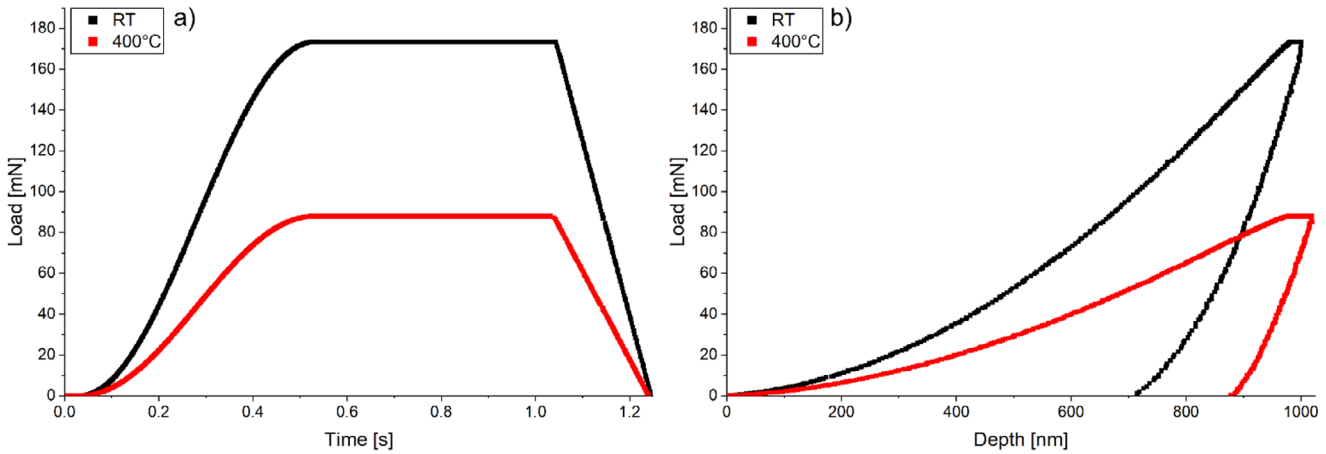


**FIGURE 2** | Representative load–time (a) and load–displacement (b) curves from HTSI measurements at room temperature (RT) and 400°C.

during the experiment. As the temperature of the sample heater is measured via a thermocouple inserted into a molybdenum spacer sheet between the heater and the sample, the sample mount temperature needs to be higher than the tip temperature to account for the thermal gradient along the thickness of the sample.

An indent with a target depth of 1000 nm was placed every minute. For each indent, the load to reach this constant depth was adjusted according to [40] to minimize the influence of size effects. The load was applied in 0.5 s following a half-sinus loading profile described in [34, 41]. After a 0.5 s holding segment at maximum load, the load was removed in 0.2 s via a continuous unloading segment. Representative load-time and load–displacement curves can be seen in Figure 2.

The unloading stiffness was determined by fitting the load ($P$)–displacement ($h$) curve as Equation (1):

$$P = A\left(h - h_f\right)^n, \tag{1}$$

according to [39], with $A$, $h_f$, and $n$ being fitting parameters. The hardness $H$ (Equation 2):

$$H = \frac{P_{\max}}{A_c}, \tag{2}$$

elastic modulus $E$ (Equation 3):

$$E = \frac{1-\upsilon^2}{\frac{1}{E_R} - \frac{1-\upsilon_{\text{tip}}^2}{E_{\text{tip}}}}, \tag{3}$$

and the coefficient of strain rate sensitivity $m$ (Equation 4):

$$m = \frac{d\ln(H)}{d\ln(\dot{\varepsilon})}, \tag{4}$$

were determined as described in [42] with the maximum load $P_{\max}$, contact area $A_c$, reduced elastic modulus $E_R$, and Poisson's ratio $\nu$. The activation volume was then calculated as Equation (5):

$$V = \frac{\sqrt{3}kT}{m\sigma_y} \approx \frac{3\sqrt{3}kT}{mH}, \tag{5}$$

[43, 44], with the Boltzmann constant $k$, absolute temperature $T$, and assuming a constraint factor of 3. This is discussed in Section 3.2.

Figure 3a shows that the target depth was reached for most tests with a deviation below 2.5%. The graph shows the depth at the end of the holding segment, so changes with increasing temperature are expected. The temperature delta ramp $dT = T_{\text{sample}} - T_{\text{tip}}$ in Figure 3b is linear over most of the tested temperature range, indicating good control of both tip and sample mount temperature. A slight oscillation is observed at temperatures below 50°C, which can be attributed to a slower initial response of the sample heater.

In addition to the HTSI measurement, continuous stiffness measurement (CSM) tests were performed at room temperature and 400°C with an indentation strain rate of $\dot{\varepsilon} = \dot{h}/h = 0.2\,s^{-1}$. The hardness and elastic modulus values obtained by the CSM measurement were averaged between depths of 750–1250 nm to be comparable to the HTSI measurements. In all CSM measurements, the hardness and elastic modulus reached an approximately constant, depth-independent value at depths above 400 nm, in line with the study by Feng and Nix [45].

After the HTSI measurement cycle, indents with a load of 1N were placed at temperatures of 150°C and 400°C, using a diamond Vickers tip (Synton-MDP AG, Nidau, Switzerland). The orientation of the indenter tip and sample was adjusted so that the edges of the indenter imprint are parallel to the edges of the sample, aligning the preferred {110}-type indentation fracture planes with the "corners" of the Vickers indent.

Supplementary strain rate jump (SRJ) nanoindentation tests [43] at room temperature were carried out using a Keysight G200 nanoindenter (Santa Rosa, CA, USA) equipped with a diamond Berkovich tip (Synton-MDP AG, Nidau, Switzerland). The indentation strain rate was varied in the order of

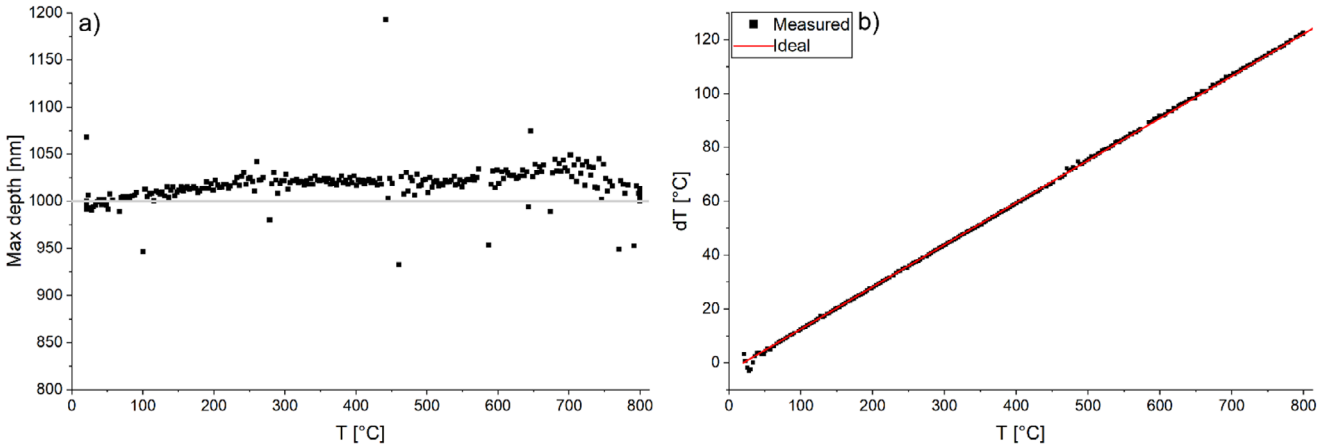


**FIGURE 3** | The maximum depth reached at the end of each test (a) and the difference between the temperature measured at the rear surface of the sample and the indenter tip (b). The ideal temperature delta is defined as starting from 0°C at a tip temperature of 20°C.

$0.05s^{-1} \rightarrow 0.005s^{-1} \rightarrow 0.05s^{-1} \rightarrow 0.001s^{-1} \rightarrow 0.05s^{-1}$ in depth increments of 300 nm.

The sample was subsequently etched with 20% aqueous sulfuric acid for 30 s [5], and etch pit analysis was performed using a TESCAN MIRA3 SEM (Brno, Czech Republic).

## 3 | Results and Discussion

In the following, the results of the HTSI measurement are presented. Each data point represents a single indent at a given temperature. The margin of error is given by the test-to-test variation and the overall width of the curves.

### 3.1 | Temperature-Dependent Mechanical Properties

The measured hardness (Figure 4a) and elastic modulus Figure 4b show a good agreement between HTSI, CSM, and literature data [29, 46, 47]. The CSM measurements show a decrease in hardness and elastic modulus from $H = 10.93 \pm 0.02$ GPa and $E = 306.8 \pm 1.8$ GPa at room temperature to $H = 5.04 \pm 0.09$ GPa and $E = 267.2 \pm 3.4$ GPa at 400°C, respectively. The elastic modulus decreases linearly with temperature, following the trend seen in $C_{11}$ by Isaak et al. [47], which will differ from the absolute values of the bulk and indentation modulus, but is proportional to E. An offset between the CSM and HTSI data is visible, which can be explained by inaccuracies in the determination of the unloading stiffness for fast unloading during thermal ramping. The hardness is only weakly affected by this.

The hardness data obtained by HTSI initially show a strong decrease with increasing temperature. The trend can be linearly described, indicated by the dashed line. At a temperature of approximately 240°C, the hardness curve starts to deviate from the linear trend. It enters a transient regime up to a temperature of approximately 400°C, above which the decrease remains linear with a lower slope until the maximum experiment temperature of 800°C, indicated by the second dashed line.

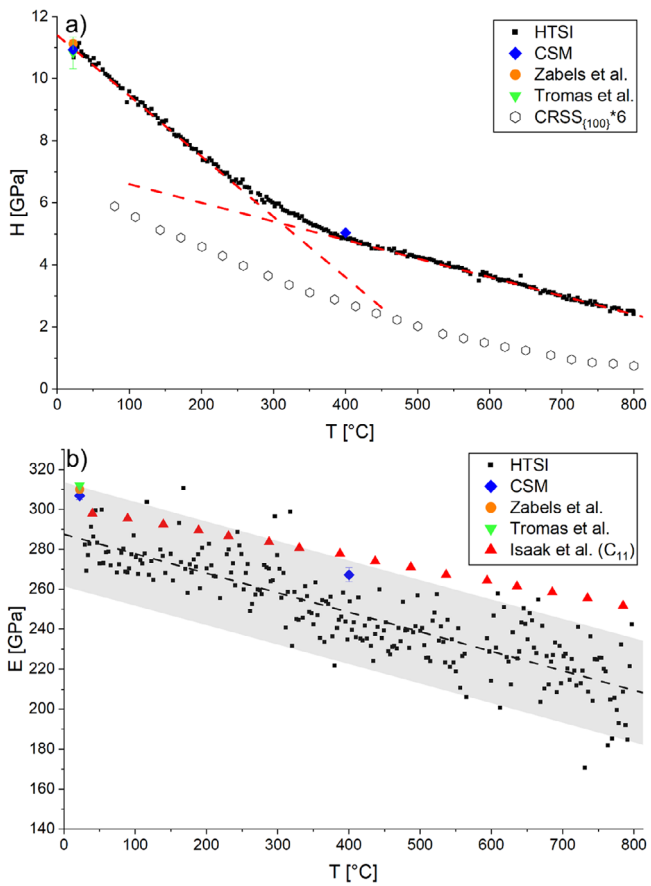


**FIGURE 4** | Measured hardness (a) and elastic modulus (b) as a function of temperature. Zabels et al. [46] and Tromas et al. [29] performed nanoindentation experiments at room temperature, while the elastic constant data by Isaak et al. [47] were obtained via rectangular parallelepiped resonance. In (a), the modeled CRSS from [48] was used for the calculation.

### 3.2 | Relating Hardness to Bulk Uniaxial Tests

The indentation hardness of MgO is significantly higher than what would usually be expected based on uniaxial tests. The

relation between uniaxial yield stress $\sigma_y$ and indentation hardness $H$ is generally discussed in terms of the constraint factor (Equation 6):

$$C_F = H/\sigma_y. \quad (6)$$

It is approximately 3 for metals [49] and assumes values between 1.5 and 4 for most materials [50]. $C_F$ depends on the yield criterion, representative strain, and elastoplastic work ratio [51–53]. As discussed in the following, the determination of a constraint factor for MgO via the comparison of uniaxial and nanoindentation tests is not trivial. In this study, a value of 3 is assumed for the calculation of the activation volume (Equation 5) by common convention [43], as changes of $C_F$ in the expected range of 2–3 do not strongly change the obtained results and do not influence their interpretation.

The uniaxial yield stress of [100]-oriented MgO is on the order of 80–100 MPa at room temperature [11, 12], which would suggest a constraint factor around 120 at first approximation. This discrepancy has already been mentioned in literature [20–22].

The high hardness of MgO can be correlated to the anisotropy of the rock salt structure and the resulting fundamentally different deformation modes under uniaxial loading and indentation. In uniaxial [100] compression, only the four 1/2<110>{110}$_{45}$ slip systems, which are inclined 45 ° to the surface (see Figure 5a), are active, while the remaining 1/2<110>{110}$_{90}$ and 1/2<110>{100} slip systems have a Schmid factor of 0. In practice, deformation is mainly localized on one or two soft 1/2<110>{110}$_{45}$ systems [54, 55]. When the compression direction is changed to [111], which only allows slip on the hard 1/2<110>{100} systems, the yield strength strongly increases by a factor of approximately 40 [13, 14] due to the significantly higher CRSS of the 1/2<110>{100} system, which reaches values beyond 1 GPa at room temperature [12, 48].

The rock salt structure possesses six physical but only two independent 1/2<110>{110} slip systems [23, 24], which are not sufficient to accommodate the complex deformation and geometrically necessary dislocations during nanoindentation. This necessitates the activation of secondary slip on other planes. Gilman and Lloyd et al. concluded that the high hardness is caused by slip on {100} planes [21, 22]. Tromas et al. [30] have observed local {211} slip via atomic force microscopy analysis of shallow indents with a depth of 20–40 nm.

The indentation hardness of MgO is therefore not directly comparable to uniaxial tests, but requires taking the hard slip systems into account. A lower-bound estimate of the hardness as $H = C_F * \sigma_y = 3 * 2 * CRSS_{\{100\}}$ [22] would be on the order of 6–9 GPa at room temperature, assuming a Schmid factor of 0.5 and not considering strain hardening in the plastic zone. In Figure 4a, this is plotted for the modelled CRSS from [48].

In the case of indenting a (100) surface, the underlying deformation therefore is a complex interplay between geometrically necessary activity on hard slip systems in the near-field and soft slip systems in the far-field. Etch pit analysis of Vickers indents (Figure 5b) shows discrete slip bands belonging to the 1/2<110>{110} slip system in the far-field, matching previously reported data [28, 56]. Both {110}$_{45}$ and {110}$_{90}$ arms can be identified, indicating that all six physical {110} systems are active [27]. The width of the slip bands shows the dislocation cross-slip capabilities. In Figure 5d, the intersections of slip lines from horizontal and vertical {110}$_{45}$ slip planes can be seen, causing local dislocation pile-up that results in the formation of cracks along {110} planes despite the natural {100} cleavage planes of MgO [28, 57, 58]. This mechanism is caused by the formation of sessile junctions via dislocation reactions (Lomer locks) [59] and subsequent pile-up from both glide planes against this obstacle.

It should be mentioned that {100} slip traces are indistinguishable from {110}$_{45}$ on the surface via the chemical etching method, and the high dislocation density close to the indentation makes the characterization of the near-field deformation difficult even in the TEM [22]. Sufficiently spaced etch pits may also be assigned to specific slip systems based on their symmetry [60], which was not achieved in this work.

### 3.3 | Thermally Activated Deformation Mechanisms

At 400°C (Figure 5c), broadening of the {110}$_{90}$ slip bands is observed, and the gap between the bands is filled with dislocations from the center, consistent with dislocation multiplication near stress concentrations like the Vickers imprint "corners". The dislocation activity is less concentrated on individual slip planes, causing the {110}$_{45}$ bands to appear significantly less pronounced and resulting in a more diffuse arrangement of dislocations around the indent. Crack nucleation via dislocation pile-up is circumvented by this higher cross-glide probability, as it allows the avoidance of obstacles like sessile junctions.

As mentioned above, the hardness of MgO is mainly governed by hard slip systems like 1/2<110>{100}, which are necessary to accommodate the near-field deformation. It is therefore reasonable to assume that its temperature dependence follows that of CRSS$_{\{100\}}$ [22].

Figure 6 shows the measured hardness change of the sample, as well as the lower-bound estimate $H = 6 * CRSS_{\{100\}}$, using the modelled CRSS from [48]. The relative changes in measured and estimated hardness, $H_{rel} = H(T)/H_0$, are in good agreement until temperatures above 400°C, where the measured hardness shows a less steep decline. This could be explained by strain hardening effects and increased dislocation densities at elevated temperatures. The results indicate that the hardness cannot be fully described by CRSS$_{\{100\}}$. The absolute value of $6 * \text{CRSS}_{\{100\}}$ is plotted in Figure 4a.

Beyond hardness, the creep segment at maximum load enables the derivation of thermal activation parameters (Figure 7). The coefficient of strain rate sensitivity $m$ initially shows values of 0.01–0.015 at room temperature, in line with the strain rate jump tests and the values reported by Golovin [61] and Messerschmidt [11]. The data points for Messerschmidt's measurements were converted from the reported flow stress and activation volume according to Equation (5). It initially decreases up to approximately 50°C, which can be attributed to the initial deviation from the thermal ramp. $m$ then linearly increases up to a temperature of 240°C, where it enters a plateau value of approximately 0.022.

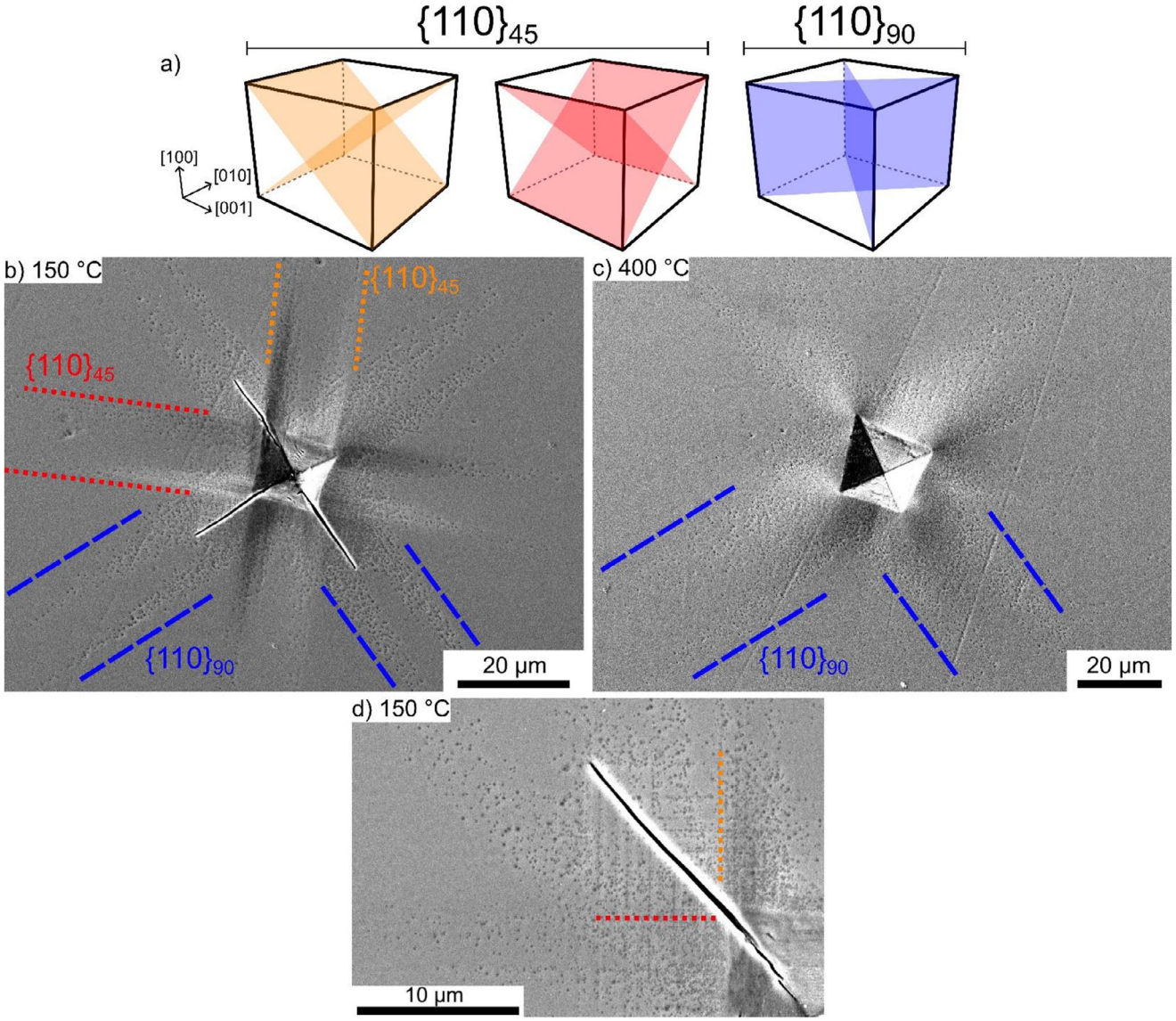


**FIGURE 5** | Top: Schematic orientations of {110} slip planes in MgO. The subscript denotes the inclination angle of the slip plane to the top surface. Bottom: SEM images of etch pits around Vickers indents at 150°C and 400°C with marked slip traces. The unmarked straight lines in (c) are small surface scratches and unrelated to the slip features.

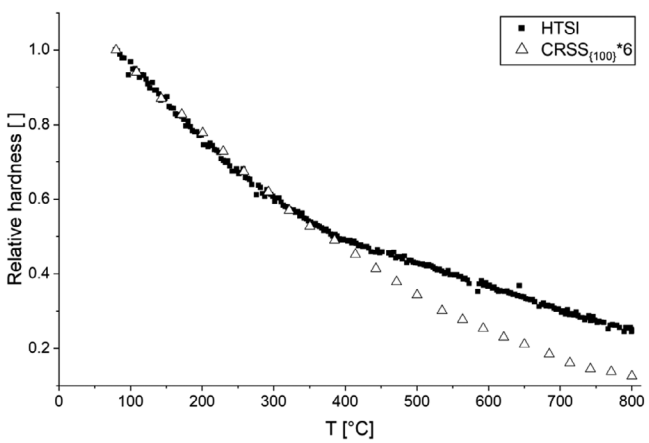


**FIGURE 6** | Relative change in hardness as a function of temperature for the experimental data and the H≈6*CRSS$_{\{100\}}$ approximation.

Above 500°C, the strain rate sensitivity increases to a peak value of 0.05 at a temperature of 675°C, above which it rapidly decreases to a value of 0.01 at the maximum temperature of 800°C.

The activation volume, derived via Equation (5), remains constant at 8–9 $b^3$ until a temperature of around 240°C, above which it slightly increases to 22 $b^3$ at 500°C. At temperatures above 675°C, the activation volume strongly increases to 80–100 $b^3$.

The bulk compression literature values for the activation volume around room temperature are much higher than in this work, on the order of 150–200 $b^3$ [7, 11]. This can be attributed to the significant difference in the stress used in this analysis. $V$ is a function of the effective stress $\sigma^*$ and increases sharply at low stresses [62–64]. As discussed previously, the local stress acting below the indenter is significantly higher than during uniaxial testing. Additionally, the high dislocation density in the plastic zone results in a smaller dislocation spacing.

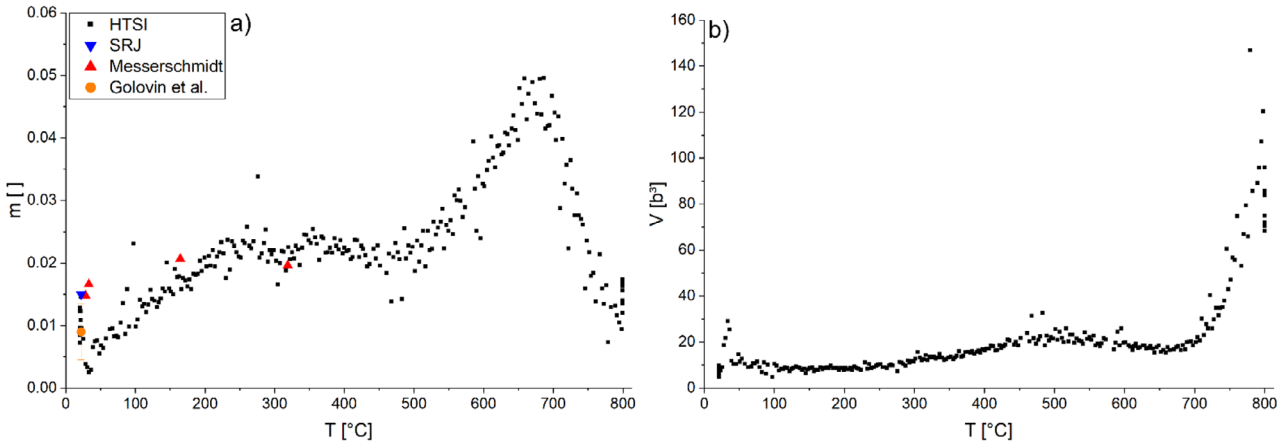


**FIGURE 7** | The coefficient of strain rate sensitivity (a) and resulting activation volume (b) as a function of temperature.

An activation volume around 10 $b^3$ is indicative of deformation via the kink pair mechanism [62, 65], while the strong increase to around 100 $b^3$ indicates long-range dislocation interaction and cross-slip [35]. At higher temperatures, above the athermal transition temperature for the {100} slip system, dislocation forest hardening is expected [66, 67], corresponding to an activation volume of several hundred $b^3$ [68]. While the trend seen in the measured data points in this direction, such high values of $V$ are not observed in the current dataset, likely due to the experiment being limited to a maximum temperature of 800°C.

### 3.4 | Correlating Hardness and Activation Parameter Regimes

The combined hardness, strain rate sensitivity, and activation volume data show a remarkable correlation to the temperature-dependent deformation regimes discussed in literature for uniaxial tests, despite the aforementioned differences:

At low to intermediate temperatures, the deformation is said to be controlled by the kink pair mechanism, which transitions to a regime governed by localized obstacles and impurity hardening [11, 18]. This transition occurs when the CRSS of the 1/2<110>{110} slip system becomes athermal. Transition temperatures between 227–327°C have been reported in literature [11, 12, 16].

This is in good agreement with the experimental nanoindentation data. At a temperature of 240°C, the hardness curve deviates from its previous linear slope. At the same temperature, the strain rate sensitivity enters a plateau.

At higher temperatures, the CRSS of the 1/2<110>{100} slip system shows a steep decrease up to a temperature of ~727°C (Figure 1b). This corresponds to the observed peak in the strain rate sensitivity. As the high temperature behavior of ceramics is comparable to the low temperature behavior of bcc metals [3], increased activation of {100} slip can be likened to the brittle-to-ductile-transition, which is indicated by a peak and subsequent decrease of the strain rate sensitivity and an increase in activation volume [69, 70], indicating a transition from thermally activated deformation via kink pairs to athermal forest hardening. This has no apparent effect on the measured hardness, affirming that the {100} glide planes already governed the hardness before this transition point.

The thermomechanical indentation behavior of MgO shows the signatures of activity on both the hard and soft slip systems. While hardness is governed by 1/2<110>{100} slip, the thermal activation parameters show clear evidence of activity on the 1/2<110>{110} slip system, indicating the significance of far-field deformation.

Further work is required to decouple the respective contributions of both slip systems quantitatively. Simulations are necessary to investigate the near-field dislocation activity on hard slip systems, while additional indentation studies can provide further insight into the influence of crystallographic orientation and tip geometry [71].

## 4 | Conclusion

Single-crystalline (100)-oriented MgO was investigated with the novel high temperature scanning indentation (HTSI) method. High-speed indents were placed while heating the sample from room temperature up to 800°C, allowing a quasi-continuous measurement of hardness, strain rate sensitivity, and activation volume. Results show:

- The decrease in hardness with increasing temperature can be expressed in terms of two linear regimes, showing a transient behavior between 240°C and 400°C.
- The strain rate sensitivity increases with increasing temperature, enters a plateau at 240°C, and shows a peak with a subsequent decrease around 675°C. The activation volume remains approximately constant at 10–20 $b^3$ until a sharp increase at temperatures above 675°C. This is in line with the expected transition temperatures from kink-pair to obstacle-controlled deformation and ultimately to long-range dislocation interactions.
- Despite the indentation hardness of MgO mainly being governed by the hard 1/2<110>{100} slip system, the observed trends in the activation parameters match the transition

temperatures expected for the different regimes in soft 1/2<110>{110} slip reported from uniaxial testing in literature.

The obtained results demonstrate that high temperature nanoindentation can serve as a powerful tool for the characterization of ductile ceramics, adding to the existing toolbox [1]. The high data density and short measurement time of the HTSI method allow a prescreening for points of interest, while the localized nature of nanoindentation also enables the future investigation of the influence of mechanically engineered dislocations [5] on temperature-dependent properties. By selecting different indenter tip geometries, dislocation nucleation and cracking behavior can also be investigated.


### Acknowledgments

We gratefully acknowledge support by the Deutsche Forschungsgemeinschaft (DFG - German Research Foundation) within the project no. DU 424/11-2 and the Open Access Publishing Fund of the Technical University of Darmstadt. O. Preuß thanks the funding for fundamental research from the European Research Council (ERC Starting Grant, Project MECERDIS, Grant Number: 101076167). Views and opinions expressed are, however, those of the authors only and do not necessarily reflect those of the European Union or the European Research Council (ERC). Neither the European Union nor the granting authority can be held responsible for them. The helpful discussions with Dr. habil. X. Fang at Karlsruhe Institute of Technology and Prof. J. Rödel at Technical University of Darmstadt are also acknowledged.

Open access funding enabled and organized by Projekt DEAL.


### Data Availability Statement

Research data associated with this article are available on the TUdatalib repository of TU Darmstadt under the DOI 10.48328/tudatalib-2268.

### References


1. A. Frisch, C. Okafor, O. Preuß, et al., "Room-Temperature Dislocation Plasticity in Ceramics: Methods, Materials, and Mechanisms," *Journal of the American Ceramic Society* 108, no. 9 (2025), https://doi.org/10.1111/jace.20575.

2. I. Słodczyk, A. Frisch, X. Fang, I. Gitman, and F. Liu, "A Data-Driven Quest for Room-Temperature Bulk Plastically Deformable Ceramics," *Journal of the American Ceramic Society* 109, no. 2 (2026), https://doi.org/10.1111/jace.70577.

3. L. Porz, "60 years of Dislocations in Ceramics: A Conceptual Framework for Dislocation Mechanics in Ceramics," *International Journal of Ceramic Engineering & Science* 4, no. 4 (2022): 214–239, https://doi.org/10.1002/ces2.10150.

4. X. Fang, A. Nakamura, and J. Rödel, "Deform to Perform: Dislocation-Tuned Properties of Ceramics," *American Ceramic Society Bulletin* 102, no. 5 (2023): 24–29.

5. O. Preuß, E. Bruder, J. Zhang, W. Lu, J. Rödel, and X. Fang, "Damage-Tolerant Oxides by Imprint of an Ultra-High Dislocation Density," *Journal of the European Ceramic Society* 45, no. 2 (2025): 116969, https://doi.org/10.1016/j.jeurceramsoc.2024.116969.

6. X. Fang, J. Zhang, A. Frisch, et al., "Room-Temperature Bulk Plasticity and Tunable Dislocation Densities in $KTaO_3$," *Journal of the American Ceramic Society* 107, no. 11 (2024): 7054–7061, https://doi.org/10.1111/jace.20040.

7. F. Appel and B. Wielke, "Low Temperature Deformation of Impure MgO Single Crystals," *Materials Science and Engineering* 73 (1985): 97–103, https://doi.org/10.1016/0025-5416(85)90299-X.

8. A. S. Argon and E. Orowan, "Plastic Deformation in MgO Single Crystals," *Philosophical Magazine* 9, no. 102 (1964): 1003–1021, https://doi.org/10.1080/14786436408211911.

9. P. Haasen, "Dislocations and the Plasticity of Ionic Crystals," *Materials Science and Technology* 1, no. 12 (1985): 1013–1024, https://doi.org/10.1179/mst.1985.1.12.1013.

10. A. E. GORUM, E. R. PARKER, and J. A. PASK, "Effect of Surface Conditions on Room-Temperature Ductility of Ionic Crystals," *Journal of the American Ceramic Society* 41, no. 5 (1958): 161–164, https://doi.org/10.1111/j.1151-2916.1958.tb13533.x.

11. U. Messerschmidt, *Dislocation Dynamics During Plastic Deformation* (Springer, 2010), https://doi.org/10.1007/978-3-642-03177-9.

12. J. Amodeo, S. Merkel, C. Tromas, et al., "Dislocations and Plastic Deformation in MgO Crystals: A Review," *Crystals* 8, no. 6 (2018): 240, https://doi.org/10.3390/cryst8060240.

13. C. O. HULSE, S. M. COPLEY, and J. A. PASK, "Effect of Crystal Orientation on Plastic Deformation of Magnesium Oxide," *Journal of the American Ceramic Society* 46, no. 7 (1963): 317–323, https://doi.org/10.1111/j.1151-2916.1963.tb11738.x.

14. S. M. Copley and J. A. Pask, "Plastic Deformation of MgO Single Crystals up to 1600°C," *Journal of the American Ceramic Society* 48, no. 3 (1965): 139–146, https://doi.org/10.1111/j.1151-2916.1965.tb16050.x.

15. R. J. Stokes, "Microstructure and Mechanical Properties of Ceramics," *Honeywell Research Center, Hopkins, MN* (1963), https://doi.org/10.21236/AD0407614.

16. P. Cordier, J. Amodeo, and P. Carrez, "Modelling the Rheology of MgO Under Earth's Mantle Pressure, Temperature and Strain Rates," *Nature* 481, no. 7380 (2012): 177–180, https://doi.org/10.1038/nature10687.

17. M. Srinivasan and T. G. Stoebe, "Temperature Dependence of Yielding and Work-Hardening Rates in Magnesium Oxide Single Crystals," *Journal of Materials Science* 9, no. 1 (1974): 121–128, https://doi.org/10.1007/BF00554762.

18. S. Takeuchi, H. Koizumi, and T. Suzuki, "Peierls Stress and Kink Pair Energy in NaCl Type Crystals," *Materials Science and Engineering: A* 521–522 (2009): 90–93, https://doi.org/10.1016/j.msea.2008.09.119.

19. F. Appel, M. Bartsch, U. Messerschmidt, E. M. Nadgornyi, and S. N. Valkovskii, "Dislocation Motion and Plasticity in MgO Single Crystals," *Physica Status Solidi (a)* 83, no. 1 (1984): 179–194, https://doi.org/10.1002/pssa.2210830120.

20. K. Sangwal, P. Gorostiza, J. Servat, and F. Sanz, "Atomic Force Microscopy Study of Nanoindentation Deformation and Indentation Size Effect in MgO Crystals," *Journal of Materials Research* 14, no. 10 (1999): 3973–3982, https://doi.org/10.1557/JMR.1999.0537.

21. J. J. Gilman, "Hardness of Pure Alkali Halides," *Journal of Applied Physics* 44, no. 3 (1973): 982–984, https://doi.org/10.1063/1.1662382.

22. S. J. Lloyd, J. M. Molina-Aldareguia, and W. J. Clegg, "Deformation Under Nanoindents in Sapphire, Spinel and Magnesia Examined Using Transmission Electron Microscopy," *Philosophical Magazine A* 82, no. 10 (2002): 1963–1969, https://doi.org/10.1080/01418610208235708.

23. G. W. Groves and A. Kelly, "Independent Slip Systems in Crystals," *Philosophical Magazine* 8, no. 89 (1963): 877–887, https://doi.org/10.1080/14786436308213843.

24. J. P. Hirth and J. Lothe, *Theory of Dislocations* (McGraw-Hill, 1968).

25. E. E. Ledoux, F. Lin, L. Miyagi , et al., "Deformation of Polycrystalline MgO up to 8.3 GPa and 1270 K: Microstructures, Dominant Slip-Systems, and Transition to Grain Boundary Sliding," *Frontiers in Earth Science* 10 (2022): 849777, https://doi.org/10.3389/feart.2022.849777.

26. K. Ishimori, S. Azuma, K. Uesugi, et al., "Temperature and Pressure Dependence on Slip Systems in MgO: Insights From Large-Strain Deformation Experiments Using the Rotational Diamond Anvil Cell," *Physics of the Earth and Planetary Interiors* 369 (2025): 107461, https://doi.org/10.1016/j.pepi.2025.107461.

27. A. S. Keh, "Dislocations in Indented Magnesium Oxide Crystals," *Journal of Applied Physics* 31, no. 9 (1960): 1538–1545, https://doi.org/10.1063/1.1735889.

28. R. W. Armstrong and C. C. Wu, "Lattice Misorientation and Displaced Volume for Microhardness Indentations in MgO Crystals," *Journal of the American Ceramic Society* 61, no. 3-4 (1978): 102–106, https://doi.org/10.1111/j.1151-2916.1978.tb09248.x.

29. C. Tromas, J. C. Girard, V. Audurier, and J. Woirgard, "Study of the Low Stress Plasticity in Single-Crystal MgO by Nanoindentation and Atomic Force Microscopy," *Journal of Materials Science* 34, no. 21 (1999): 5337–5342, https://doi.org/10.1023/A:1004705206482.

30. C. Tromas, J. C. Girard, and J. Woirgard, "Study by Atomic Force Microscopy of Elementary Deformation Mechanisms Involved in Low Load Indentations in MgO Crystals," *Philosophical Magazine A* 80, no. 10 (2000): 2325–2335, https://doi.org/10.1080/01418610008216475.

31. J. H. Hensler and G. V. Cullen, "Stress, Temperature, and Strain Rate in Creep of Magnesium Oxide," *Journal of the American Ceramic Society* 51, no. 10 (1968): 557–559, https://doi.org/10.1111/j.1151-2916.1968.tb13321.x.

32. J. Routbort, "Work Hardening and Creep of MgO," *Acta Metallurgica* 27, no. 4 (1979): 649–661, https://doi.org/10.1016/0001-6160(79)90016-6.

33. O. A. Ruano, J. Wolfenstine, J. Wadsworth, and O. D. Sherby, "Harper–Dorn and Power-Law Creep in Single-Crystalline Magnesium Oxide," *Journal of the American Ceramic Society* 75, no. 7 (1992): 1737–1741, https://doi.org/10.1111/j.1151-2916.1992.tb07190.x.

34. G. Tiphéne, P. Baral, S. Comby-Dassonneville, et al., "High-Temperature Scanning Indentation: A New Method to Investigate in Situ Metallurgical Evolution Along Temperature Ramps," *Journal of Materials Research* 36, no. 12 (2021): 2383–2396, https://doi.org/10.1557/s43578-021-00107-7.

35. H. Conrad, "Thermally Activated Deformation of Metals," *Jom Journal of the Minerals, Metals and Materials Society* 16, no. 7 (1964): 582–588, https://doi.org/10.1007/BF03378292.

36. J. Wheeler, V. Maier, K. Durst, M. Göken, and J. Michler, "Activation Parameters for Deformation of Ultrafine-Grained Aluminium as Determined by Indentation Strain Rate Jumps at Elevated Temperature," *Materials Science and Engineering: A* 585 (2013): 108–113, https://doi.org/10.1016/j.msea.2013.07.033.

37. K. Durst and V. Maier, "Dynamic Nanoindentation Testing for Studying Thermally Activated Processes From Single to Nanocrystalline Metals," *Current Opinion in Solid State and Materials Science* 19, no. 6 (2015): 340–353, https://doi.org/10.1016/j.cossms.2015.02.001.

38. C. Minnert, W. C. Oliver, and K. Durst, "New Ultra-High Temperature Nanoindentation System for Operating at up to 1100°C," *Materials & Design* 192 (2020): 108727, https://doi.org/10.1016/j.matdes.2020.108727.

39. W. C. Oliver and G. M. Pharr, "An Improved Technique for Determining Hardness and Elastic Modulus Using Load and Displacement Sensing Indentation Experiments," *Journal of Materials Research* 7, no. 6 (1992): 1564–1583, https://doi.org/10.1557/JMR.1992.1564.

40. G. Tiphéne, B. Adogou, G. Guillonneau, et al., "Update of the HTSI Method: Application to the Characterization of Mechanical Properties of $CaF_2$ From RT to 800°C," *Journal of Materials Research* 39 (2024): 3329–3344, https://doi.org/10.1557/s43578-024-01466-7.

41. G. Tiphéne, *High-Temperature Scanning Indentation (HTSI): Compréhension Des Essais de Nanoindentation Lors Des Transformations Physiques de Matériaux Métalliques à Haute Température* (École Centrale de Lyon, 2023), https://theses.hal.science/tel-04117610/.

42. M. Sos, G. Tiphene, J. Loubet, S. Bruns, E. Bruder, and K. Durst, "Mechanical Softening of CuX Alloys at Elevated Temperatures Studied via High Temperature Scanning Indentation," *Materials & Design* 240 (2024): 112865, https://doi.org/10.1016/j.matdes.2024.112865.

43. V. Maier, K. Durst, J. Mueller, B. Backes, H. W. Höppel, and M. Göken, "Nanoindentation Strain-Rate Jump Tests for Determining the Local Strain-Rate Sensitivity in Nanocrystalline Ni and Ultrafine-Grained Al," *Journal of Materials Research* 26, no. 11 (2011): 1421–1430, https://doi.org/10.1557/jmr.2011.156.

44. V. Maier-Kiener and K. Durst, "Advanced Nanoindentation Testing for Studying Strain-Rate Sensitivity and Activation Volume," *Jom Journal of the Minerals, Metals and Materials Society* 69, no. 11 (2017): 2246–2255, https://doi.org/10.1007/s11837-017-2536-y.

45. G. Feng and W. D. Nix, "Indentation Size Effect in MgO," *Scripta Materialia* 51, no. 6 (2004): 599–603, https://doi.org/10.1016/j.scriptamat.2004.05.034.

46. R. Zabels, I. Manika, K. Schwartz, et al., "Depth Profiles of Indentation Hardness and Dislocation Mobility in MgO Single Crystals Irradiated With Swift 84Kr and 14N Ions," *Applied Physics A* 120, no. 1 (2015): 167–173, https://doi.org/10.1007/s00339-015-9145-9.

47. D. Isaak, O. Anderson, and T. Goto, "Measured Elastic Moduli of Single-Crystal MgO up to 1800 K," *Springer Nature* 16, no. 7 (1989): 704–713, https://doi.org/10.1007/BF00223321.

48. J. Amodeo, P. Carrez, B. Devincre, and P. Cordier, "Multiscale Modelling of MgO Plasticity," *Acta Materialia* 59, no. 6 (2011): 2291–2301, https://doi.org/10.1016/j.actamat.2010.12.020.

49. D. Tabor, "Indentation Hardness: Fifty Years on a Personal View," *Philosophical Magazine A* 74, no. 5 (1996): 1207–1212, https://doi.org/10.1080/01418619608239720.

50. A. Clausner and F. Richter, "Determination of Yield Stress From Nano-indentation Experiments," *European Journal of Mechanics—A/Solids* 51 (2015): 11–20, https://doi.org/10.1016/j.euromechsol.2014.11.008.

51. M. Sakai, T. Akatsu, S. Numata, and K. Matsuda, "Linear Strain Hardening in Elastoplastic Indentation Contact," *Journal of Materials Research* 18, no. 9 (2003): 2087–2096, https://doi.org/10.1557/JMR.2003.0293.

52. S. Shim, J. Jang, and G. Pharr, "Extraction of Flow Properties of Single-Crystal Silicon Carbide by Nanoindentation and Finite-element Simulation," *Acta Materialia* 56, no. 15 (2008): 3824–3832, https://doi.org/10.1016/j.actamat.2008.04.013.

53. A. Leitner, V. Maier-Kiener, and D. Kiener, "Essential Refinements of Spherical Nanoindentation Protocols for the Reliable Determination of Mechanical Flow Curves," *Materials & Design* 146 (2018): 69–80, https://doi.org/10.1016/j.matdes.2018.03.003.

54. R. B. Day and R. J. Stokes, "Mechanical Behavior of Magnesium Oxide at High Temperatures," *Journal of the American Ceramic Society* 47, no. 10 (1964): 493–503, https://doi.org/10.1111/j.1151-2916.1964.tb13797.x.

55. C. O. Hulse and J. A. Pask, "Mechanical Properties of Magnesia Single Crystals Corn Pression," *Journal of the American Ceramic Society* 43, no. 7 (1960): 373–378, https://doi.org/10.1111/j.1151-2916.1960.tb13674.x.

56. J. Woirgard, C. Tromas, J. Girard, and V. Audurier, "Study of the Mechanical Properties of Ceramic Materials by the Nanoindentation Technique," *Journal of the European Ceramic Society* 18, no. 15 (1998): 2297–2305, https://doi.org/10.1016/S0955-2219(98)00083-1.

57. A. S. Keh, "Cracks Due to the Piling-up of Dislocations on Two Intersecting Slip Planes in MgO Crystals," *Acta Metallurgica* 7, no. 10 (1959): 694–696, https://doi.org/10.1016/0001-6160(59)90156-7.

58. M. M. Chaudhri, "The Displacement of Material and the Formation of $\{1\bar{1}0\}_{90}$, Cracks Around Spherical Indentations in MgO Crystals," *Philosophical Magazine A* 53, no. 4 (1986): L55–L63, https://doi.org/10.1080/01418618608242844.

59. P. Carrez, P. Cordier, B. Devincre, and L. P. Kubin, "Dislocation Reactions and Junctions in MgO," *Materials Science and Engineering: A* 400–401 (2005): 325–328, https://doi.org/10.1016/j.msea.2005.03.071.

60. F. Javaid, A. Stukowski, and K. Durst, "3D Dislocation Structure Evolution in Strontium Titanate: Spherical Indentation Experiments and MD Simulations," *Journal of the American Ceramic Society* 100, no. 3 (2017): 1134–1145, https://doi.org/10.1111/jace.14626.

61. Y. I. Golovin, Y. L. Iunin, and A. I. Tyurin, "Strain-rate Sensitivity of the Hardness of Crystalline Materials Under Dynamic Nanoindentation," *Doklady Physics* 48, no. 9 (2003): 505–508, https://doi.org/10.1134/1.1616061.

62. M. N. Sinha, D. J. Lloyd, and K. Tangri, "Dislocation Dynamics and Thermally-Activated Deformation of MgO Single Crystals," *Philosophical Magazine* 28, no. 6 (1973): 1341–1352, https://doi.org/10.1080/14786437308228003.

63. J. Kubát and M. Rigdahl, "The Exponential and Power Laws of Stress Relaxation Kinetics and a General Relation Between the Activation Volume and Effective Stress," *Physica Status Solidi (a)* 35, no. 1 (1976): 173–180, https://doi.org/10.1002/pssa.2210350119.

64. G. Taylor, "Thermally-activated Deformation of BCC Metals and Alloys," *Progress in Materials Science* 36 (1992): 29–61, https://doi.org/10.1016/0079-6425(92)90004-Q.

65. J. E. Dorn and S. Rajnak, "Nucleation of Kink Pairs and the Peierls′ mechanism of Plastic Deformation. *LBNL Report* 1963, UCRL-10833," .

66. J. Amodeo, B. Devincre, P. Carrez, and P. Cordier, "Dislocation Reactions, Plastic Anisotropy and Forest Strengthening in MgO at High Temperature," *Mechanics of Materials* 71 (2014): 62–73, https://doi.org/10.1016/j.mechmat.2014.01.001.

67. J. Amodeo, S. Dancette, and L. Delannay, "Atomistically-Informed Crystal Plasticity in MgO Polycrystals Under Pressure," *International Journal of Plasticity* 82 (2016): 177–191, https://doi.org/10.1016/j.ijplas.2016.03.004.

68. S. Mishra, V. K. Beura, A. Singh, and M. Yadava, "A Perspective on Strain Hardening Behavior of Materials Considering Mobile Dislocation Density and Activation Volume," *Metallurgical and Materials Transactions A* 50, no. 8 (2019): 3472–3477, https://doi.org/10.1007/s11661-019-05316-8.

69. D. Kiener, R. Fritz, M. Alfreider, A. Leitner, R. Pippan, and V. Maier-Kiener, "Rate Limiting Deformation Mechanisms of Bcc Metals in Confined Volumes," *Acta Materialia* 166 (2019): 687–701, https://doi.org/10.1016/j.actamat.2019.01.020.

70. C. Minnert, H. ur Rehman, and K. Durst, "Thermally Activated Dislocation Mechanism in Mo Studied by Indentation, Compression and Impact Testing," *Journal of Materials Research* 36, no. 12 (2021): 2397–2407, https://doi.org/10.1557/s43578-021-00126-4.

71. A. Richter, B. Wolf, M. Nowicki, et al., "Multi-Cycling Nanoindentation in MgO Single Crystals Before and After Ion Irradiation," *Journal of Physics D: Applied Physics* 39, no. 15 (2006): 3342–3349, https://doi.org/10.1088/0022-3727/39/15/018.